International Journal of Control, Automation and Systems 18(1) (2020) 53-64
http://dx.doi.org/10.1007/s12555-019-0238-7
ISSN:1598-6446 eISSN:2005-4092
http://www.springer.com/12555

Manufacturing and Control of a Robotic Device for Time-averaged Simulated Micro and Partial Gravity of a Cell Culture Environment

Yoon Jae Kim, Min Hyuk Lim, Byoungjun Jeon, Dong Hyun Choi, Haeri Lee, Ae Jin Jeong, Min Jung Kim, Ji Won Park, Ja-Lok Ku, Seung-Yong Jeong, Sang-Kyu Ye, Youdan Kim, and Sungwan Kim*

Abstract: Gravity is omnipresent for all objects on Earth. However, in an environment of different gravitational stress (e.g., microgravity or partial gravity), cells and organs show different biological responses. So, researchers have attempted to achieve micro- or partial gravity on Earth through various approaches, such as parabolic flight or free fall. However, the duration of such ground experiments is highly limited, making it very difficult to conduct time-consuming tasks, such as cell culture. Thus, a three-dimensional (3D) clinostat is utilized as an alternative for experiments on the International Space Station. It provides time-averaged simulated micro- and partial gravity by using mechanical frames with two rotating actuators. This study proposes novel control algorithms for simulating micro- and partial gravity and validates them by applying it to the control of a manufactured 3D clinostat. First, the novel algorithm for time-averaged simulated microgravity (taSMG) provided a more uniformly distributed gravity field by reducing two poles the gravity-concentrated areas. The taSMG with reduced poles provides isotropic gravitational patterns, from which it is possible to minimize the unnecessary effect due to nonuniformity of the gravity vector direction. Second, the other suggested novel algorithm for time-averaged simulated partial gravity (taSPG) controls the pole sizes asymmetrically to generate the intended size of partial gravity. The suggested algorithms are based on mathematical models rather than totally randomized motions. Therefore, the convergence of gravity values, in the rotating frame over time, can be analytically predicted with improved accuracy compared with previously reported algorithms. The developed 3D clinostat hardware and algorithms will effectively provide well-validated taSMG and taSPG for cell growth experiments in future studies for space medicine.

Keywords: Cell culture, clinostat, control algorithm, microgravity, partial gravity, space medicine.

1. INTRODUCTION

Gravity is an omnipresent force on Earth that constantly influences all living things on the ground. Since the 1960s, astronauts exposed to long-term microgravity have shown various physiological changes, such as abnormal cellular functions, immune dysregulation, and muscle atrophy [1–8]. Therefore, many researchers have attempted to identify the effects of these changes under microgravity. However, experiments on the International Space Station (ISS) are very expensive and are not easily permitted for general researchers. On the ground, physical microgravity can be achieved by free fall from a drop tower or parabolic flight. However, the non-stress duration is too short to conduct cell cultivation. Thus, researchers have attempted to produce practically feasible gravitational stress that can provide a similar biological effect on living things.

Time-averaged simulated microgravity (taSMG) has been suggested as an alternative method and validated by comparing the biological effect with that on the ISS [9–13]. Previous studies validated that specific types of cells, such as leukocytes [9, 10] and T lymphocytes

Manuscript received April 1, 2019; revised August 4, 2019; accepted August 13, 2019. Recommended by Guest Editors Doo Yong Lee (KAIST) and Jaesoon Choi (Asan Medical Center). This work was supported by the National Research Foundation of Korea (NRF) funded by the Korea government (NRF-2018M1A3A3A02065779).

Yoon Jae Kim is with the Institute of Medical and Biological Engineering, Seoul National University (SNU), Seoul 03080, Korea (e-mail: yoonjaekim@snu.ac.kr). Min Hyuk Lim (co-first author), Dong Hyun Choi, and Sungwan Kim are with the Department of Biomedical Engineering, SNU College of Medicine, Seoul 03080, Korea (e-mails: minhyuk@snu.ac.kr, donghyun369@naver.com, sungwan@snu.ac.kr). Byoungjun Jeon is with the Interdisciplinary Program for Bioengineering, SNU, Seoul 03080, Korea (e-mail: bjjeon125@gmail.com). Haeri Lee, Ae Jin Jeong, and Sang-Kyu Ye are with the Department of Pharmacology and Biomedical Sciences, SNU College of Medicine, Seoul 03080, Korea (e-mails: hrlee519@gmail.com, love89@snu.ac.kr, sangkyu@snu.ac.kr). Min Jung Kim and Ji Won Park are with the Department of Surgery, Seoul National University Hospital, Seoul 03080, Korea (e-mails: surgeon.mjkim@gmail.com, sowisdom@gmail.com). Ja-Lok Ku is with the Department of Biomedical Sciences, SNU College of Medicine, Seoul 03080, Korea (e-mail: kujalok@snu.ac.kr). Seung-Yong Jeong is with the Department of Surgery, SNU College of Medicine, Seoul 03080, Korea (e-mail: syjeong@snu.ac.kr). Youdan Kim is with the Department of Mechanical and Aerospace Engineering, SNU College of Engineering, Seoul 08826, Korea (e-mail: ydkim@snu.ac.kr).
* Corresponding author.

[11–13], show similar growing results when exposed to physical microgravity and taSMG. taSMG can be generated by a novel mechanical device, called the 3D clinostat [14]. The 3D clinostat consists of two motors with perpendicular axes. The outer frame is rotated by an actuator, while the inner frame is rotated by another actuator fixed to the outer frame. The target cells can be fixed and grown at the inner frame, where they are exposed to gravity cancellation over time.

A variety of gravity cancellations occur depending on how the two actuators are controlled. Diverse control algorithms, suggested in previous studies, provide different gravity patterns [15]. Most conventional algorithms provide taSMG by rotating two axes with a constant angular velocity [16, 17] or a constant angular velocity but with a direction inverted at a randomly chosen time [15, 18]. However, these algorithms do not provide a uniform gravity distribution because gravity-focused areas, such as poles, are formed on opposite sides [19]. Even though the gravity vectors of the pole at the opposite side cancel the vectors to the poles over time, it causes an uneven gravity distribution. This has the potential to cause unpredictable effects on the cells, due to the irregularity of gravity affecting the cells. To overcome the weakness of conventional algorithms, the random walk algorithm was applied to the 3D clinostat, which eliminated the existence of poles [19]. This group expanded the random walk algorithm to control unevenly sized poles, in which the time-averaged simulated partial gravity (taSPG) is realized. Furthermore, it was also possible to continuously change the direction of the poles by using an additional third actuator for a clinostat [20]. The continuous change in pole location can prevent the generation of gravity-focused areas. However, introducing a third actuator is inefficient, in terms of design, and the overall hardware size and weight will increase. Additionally, rapid changes in rotating direction could lead to unpredictable results in cell culture because of external accelerations based on the impact responses from the random walk algorithm. Thus, previous clinostats have tried to overcome these shortcomings by using two actuators and a complicated algorithm.

Compared with real microgravity, taSMG has a similar effect on cells and organs only in a very few instances. However, the value of taSMG lies in the fact that it is not limited to similarity with real microgravity. Diverse gravitational patterns, provided by the 3D clinostat with various algorithms, can cause changes in the cell signaling pathway, which is expected to have several positive effects. Various biological changes in cell metabolism, under certain gravitational stresses, are expected to be adopted for biological and medical investigations. A recent study [16, 17] reported that the growth of Hodgkin's lymphoma cells (a type of cancer cell) was selectively inhibited by autophagy, whereas normal human dermal fibroblast was not affected by the stress in taSMG environments. This suggests the need to study the physiological changes exhibited by cells within various gravitational patterns, because these observations can be utilized to improve various medical treatments.

In this study, 3D clinostat hardware was manufactured and two novel control algorithms were proposed and implemented to generate improved environments of taSMG and taSPG, respectively. The suggested algorithms are based on mathematical models instead of totally randomized motions, so they provide predictable time-averaged gravity as time passes. This provides more controlled cell cultivation at taSMG and taSPG, whereas algorithms of recent studies depended on random walk motion. A 5-h validation was then performed to confirm the agreement between the analytically predicted and actual time-averaged gravity values.

2. HARDWARE MANUFACTURING

The manufactured 3D clinostat consisted of three parts: the inner frame, outer frame, and a supporter. A rotary actuator was fixed on the supporter to transmit torque to the outer frame using two identical gears. The inner frame was connected to the outer frame. The rotation axis of the inner frame was perpendicular to the that of the outer frame. The inner frame contained a stage to grow cells and was rotated by a second rotary actuator. A Dynamixel (MX-64AT, ROBOTIS, Gangseo-gu, Seoul, Korea) was used for the actuators, which were controlled by an ATMega 2561-based controller (CM-700, ROBOTIS). Power and communication lines were connected from the actuator of the inner frame to the actuator of the outer frame; and then from the actuator of the outer frame to the controller. To connect the lines between the two actuators of the inner and outer frames, a slip ring (SNH012-08S, SENRING, SongGang, ShenZhen, China) with a shaft hole was used to prevent twisting of the line. This is superior to conventional slip rings because it can connect electrical wires and the rotating shaft simultaneously. Power was supplied by an SMPS (12V-5A model, DEE VAN ENTERPRISE, Hsin-Tien City, Taipei, Taiwan) via the controller. The control algorithm could be downloaded to the controller using a USB downloader (LN-101, ROBOTIS). A USB communication converter (U2D2, ROBOTIS) and a power converter (SMPS2 Dynamixel, ROBOTIS) were used when the actuators were controlled by a PC.

Proper bearings were used to ensure sufficient durability, considering that the clinostat would be used in a repetitive and long-term experiment. Two radial bearings were used for the outer frame rotation. Meanwhile, two radial bearings and a thrust bearing were used for the inner frame rotation. Details of the mechanical and electrical components are listed in Table 1. Fig. 1 shows the complete 3D clinostat hardware. The detailed dimensions of the 3D cli-

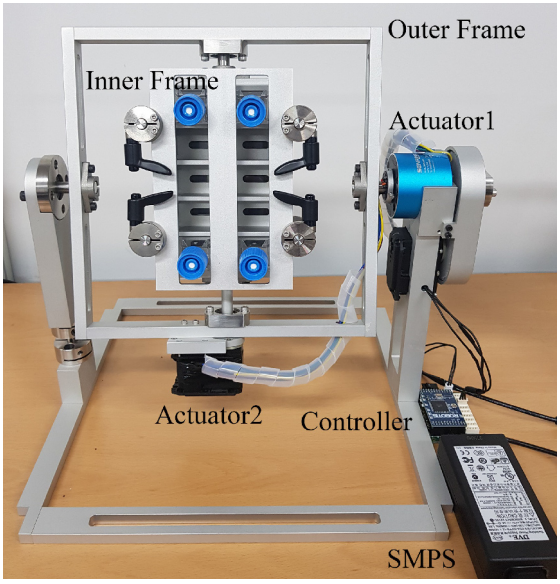

Fig. 1. 3D clinostat hardware.

nostat were designed to fit into a standard incubator.

In the case of control using the controller, the algorithm can be coded using commercial software (R+ Task 2.0, ROBOTIS). For control using the PC, a C-based dynamic-link library and a MATLAB-based software development kit (SDK) are used. The experiment of this study was PC-controlled and the detailed algorithm was coded with MATLAB. The proposed algorithms of this study can be intuitively implemented with introduced equations and paragraphs in the CONTROL ALGORITHM section.

3. CONTROL ALGORITHM

3.1. Control overview

Three types of algorithms were applied. Algorithm 1 presents a conventional approach that provides taSMG. The results of Algorithm 1 can be used as the control group for the evaluation of Algorithms 2 and 3. Algorithm 2 overcomes the pole issue of the conventional approach by rotating faster at the pole area. Algorithm 3 provides the taSPG by using a mathematical model. Proportional-derivative (PD) control is applied to solve the practical issue of using a motor to implement the suggested model. Even though the previously reported random walk algorithm [17] enabled both taSMG (without poles) and taSPG, the proposed algorithms can be more effective with faster gravity cancellation and can pursue smooth patterns for preventing impact responses, since the algorithm that controls the gravity vector is based on a mathematical model instead of total randomness.

Table 1. Mechanical and electrical components.

Component	Model	Manufacturer	Specification
Actuator	MX-64AT	ROBOTIS	Weight: 135 g Resolution: 4,096 steps (0.0879°/step) Stall torque: 6 Nm
Controller	CM-700	ROBOTIS	Weight: 37.3 g CPU: ATMega2561 Voltage: 7 V-35 V Environment Temperature: $-5°C$-$70°C$
Slip ring	SNH012-08S	SENRING	-
SMPS	12V-5A	DEE VAN ENTERPRISE	-
USB downloader	LN-101	ROBOTIS	-
USB communication cable	U2D2	ROBOTIS	Weight: 9 g Communication: TTL/RS-485/UART Transmission speed: Max. 6 Mbps
Power converter	SMPS2 Dynamixel	ROBOTIS	-
Radial bearing	SBGTA 6900ZZ	MISUMI	Inner diameter: 10 mm Bearing material: Stainless steel Holder material: SUS304
	brdn 2610	MISUMI	Inner diameter: 10 mm Bearing material: Steel Holder material: S45C
Thrust bearing	F6-14M	MISUMI	Inner diameter: 6 mm Outer diameter: 14 mm Material: Steel

3.2. Algorithm 1: taSMG

As the simplest algorithm, the two axes can be rotated with the velocity profile of a random distribution. The outer actuator provided the velocity profile of a uniform random distribution from 0.0600 to 0.0959 rad/s. The inner actuator provided the velocity profile of a uniform random distribution from 0.0959 to 0.1318 rad/s. Randomness was included to provide random variation of the gravity vector trajectory, regardless of whether it eliminates the poles or not.

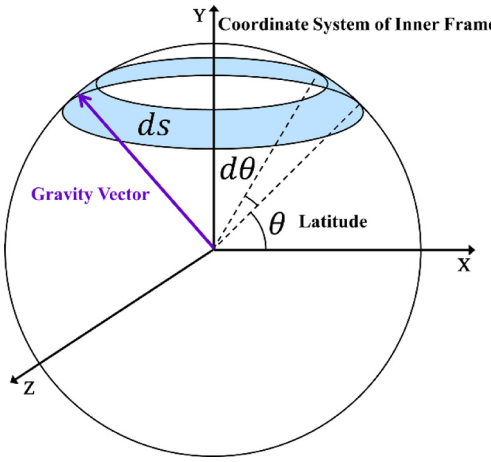

Fig. 2. Latitude of the gravity vector at the coordinate system of the inner frame.

3.3. Algorithm 2: taSMG with reduced poles

As the second algorithm, a novel concept was added to overcome the limitation of Algorithm 1 (Fig. 1). Actuator 1 controlled the latitude of the gravity vector, while Actuator 2 controlled the longitude of the gravity vector. As shown in Fig. 2, a pole was generated because the micro area (ds) assigned to each latitude reduces as the latitude increases. Therefore, at an area with a higher latitude, Actuator 1 should rotate faster to reduce the gravity vector accumulation.

Actuator 2, which controlled the longitude of the gravity vector, was operated in the same manner as Algorithm 1, with randomness. The micro area of latitude θ (Fig. 2) for Actuator 1 is expressed in (1) as follows:

$$ds = 2\pi r^2 \cos\theta d\theta, \tag{1}$$

$$w(\theta) = \min\left(\frac{k}{\|\cos\theta\|}, w_{max}\right). \tag{2}$$

The micro area ds is proportionate to $\cos\theta$. Thus, angular velocity w was designed to be inversely proportional to $\cos\theta$. This is because the duration for which the gravity vectors stay at a certain latitude, must be proportional to the micro area at that latitude. By this design, the staying time at each latitude was forced to be nearly uniform, and thus the irregularity of simulating gravity patterns was expected to be reduced. In this study, k and w_{max} were set to 0.119834 rad/s and 1.19834 rad/s, respectively, by considering the specificity of the applied Dynamixel model.

3.4. Algorithm 3: taSPG

Partial gravity, which is defined as the gravity between microgravity and 1g, is present on the Moon (0.17 g) or Mars (0.38 g). The novel concept of Algorithm 3 for taSPG is suggested and implemented herein. taSPG can be achieved by making the sizes of the two poles different. As mentioned in Algorithm 2, the pole size was reduced in the case where the angular velocity near the pole was fast. Conversely, when the speed was lower near the pole, the pole size increased. In this way, the difference in the size of both poles could be controlled, and taSPG could be realized by preventing gravity vectors of poles from being cancelled.

The difference between the two poles was controlled based on the velocity profile suggested in (3).

$$w(t) = w_0 - \alpha w_0 \cos(w_0 t), \tag{3}$$

$$\theta(t) = w_0 t - \alpha \sin(w_0 t) + \theta_0. \tag{4}$$

At the initial condition ($t = 0$), the axis of Actuator 2 should be aligned parallel to the gravitational field. The rotated angle θ is defined as the angle between the axis of Actuator 2 and the gravitational field (note: definitions of θ at Algorithm 2 and 3 are different, $\theta_0 = 0$). At $\theta = 2n\pi$ ($n = 0, 1, 2, \ldots$), w was at its minimum (large pole), and at $\theta = (2n+1)\pi$ ($n = 0, 1, 2, \ldots$), w was at its maximum (small pole). Parameter α was a constant value from 0 to 1. When α was 0, w became a constant value, and taSMG was generated. When α was 1, the difference of w at large and small poles was at their maximum, while the value of the taSPG reached its maximum. Theoretically, based on the suggested velocity profile, taSPG can be implemented as follows (5):

$$\text{taSPG} = \frac{1}{T}\int_0^T g\cos(w_0 t - \alpha\sin(w_0 t))dt, \tag{5}$$

where T is the time of a cycle calculated as $2\pi/w_0$. In this study, 9.8 m/s^2 was adopted as the g value, and α was set to 1 to identify the maximum taSPG. The theoretical value was calculated using a numerical approach to be compared with the actual operation results of the 3D clinostat.

In considering the practical control issues, angular velocity control to follow the velocity profile of (3) was not achieved with an open-loop system. For the control of the Dynamixel, the time latency, discontinuous control command (approximately 30 Hz), and limited resolution of the angular velocity increment (0.0119834 rad/s) rendered the proposed strategy to accumulate error in the positions of the poles. Furthermore, the low resolution of the commandable angular velocity increment made real-time angular velocity control inapplicable. Thus, the pole position error, which is defined by difference of the angles in the directions between theoretical and measured gravity vectors, was used for the closed-loop feedback.

Now, equation (3) is modified to the below (6) where w_1 is the practical angular velocity near w_0 to orient the large pole toward the desired direction at $\theta = 2n\pi$ ($n = 0, 1, 2, \ldots$).

$$w(t) = w_0 - \alpha w_0 \cos(w_1 t). \tag{6}$$

Fig. 3 shows the block diagram of the proposed control approach. Basically, the angular velocity w, calculated

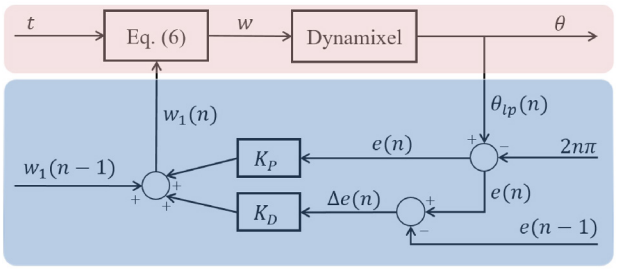

Fig. 3. Block diagram of the control flow. The blue box is activated only when gravity vector reaches at the large pole.

by (6), is the input to Dynamixel as depicted inside the red box in Fig. 3. The control flow inside the blue box is activated only when the gravity vector reaches at the large pole $\theta(t) = \theta_{lp}(n)$ where n is the number of cycles. Theoretically, the large pole, the point at which the Dynamixel's angular velocity is the slowest, should be formed at the point where $\theta = 2n\pi$ according to (3). The angle of the large pole $\theta_{lp}(n)$ is measured and $2n\pi$ (desired position of large pole) is subtracted to compute the error of the large pole position $e(n)$ as shown in (7). A positive error indicates that the pole position lies ahead of the desired position, while a negative error indicates that the pole position is behind the desired position. The pole position error was compensated by modification of parameter w_1. The error $e(n)$ and the difference of error $\Delta e(n)$ are calculated as (7) and (8). Then, w_1 is updated with proportional and differential gains as represented in (9). When the error is positive, w_1 is increased to follow the velocity profile (3) faster. When the error is negative, w_1 decreased to follow the velocity profile slower. The initial condition of $w_1(0)$ was set to w_0 as shown in (10).

$$e(n) = \theta_{lp}(n) - 2n\pi, \tag{7}$$

$$\Delta e(n) = e(n) - e(n-1), \tag{8}$$

$$w_1(n) = w_1(n-1) + K_P e(n) + K_D \Delta e(n), \tag{9}$$

where

$$w_1(0) = w_0. \tag{10}$$

3.5. Validation

The three algorithms were applied to control the 3D clinostat using the MATLAB SDK. Each algorithm was applied for 5 h. The gravity was measured using a sensor with a sampling frequency of 50 Hz. In the case of Algorithm 3, the taSPG value measured by the sensor was compared with the numerically derived theoretical value.

4. RESULTS

4.1. Algorithm 1: taSMG

Algorithm 3 was applied to the 3D clinostat for 5 h. Fig. 4(b) shows the gravity vector distribution from measurement. The figure depicts two poles, where the gravity vectors are significantly focused. Areas with almost no gravitational vectors were also identified, showing a generally uneven gravity distribution. In Figs. 4(a) and (b), two poles are along with y-axis, which is parallel to the axis of Actuator 2. Fig. 5(a) illustrates the x, y, and z components of the time-averaged simulated gravity as time passed. The green lines in Figs. 5(a) and (b) depict the normed gravitational acceleration after 1 h and 5 h, respectively. The results are also summarized in Table 2. The convergence rate shows the progress from initial value to target value. The time-averaged value approached 0.121 m/s^2 (0.0124 g) after the 5 h operation. Although the value sometimes decreased, no further significant improvement was expected.

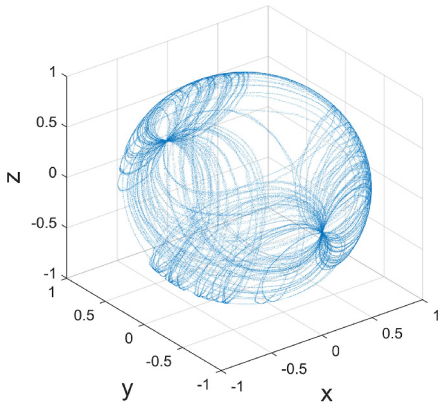

(a)

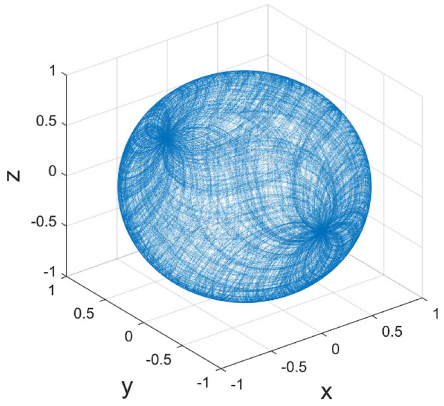

(b)

Fig. 4. Gravity distribution generated by Algorithm 1 for (a) 1 h and (b) 5 h.

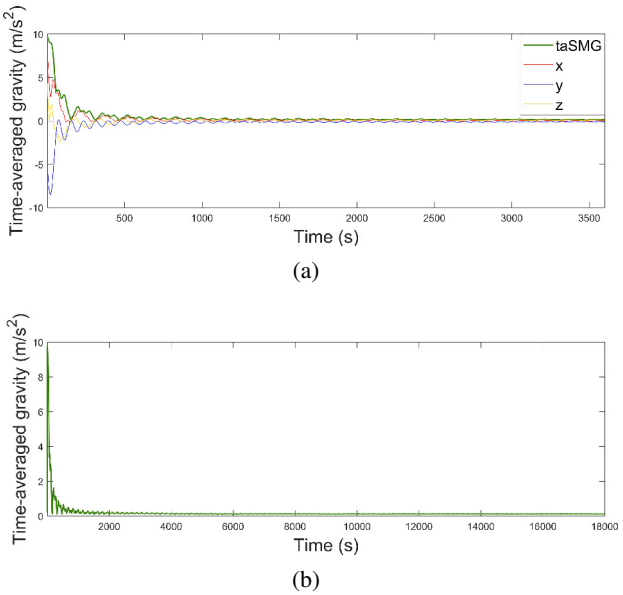

Fig. 5. Time-averaged simulated microgravity generated by Algorithm 1. (a) represents taSMG and its x, y, and z components for 1 h. (b) represents taSMG for 5 h.

Table 2. taSMG and convergence rate over time (Algorithm 1).

Time (s)	60	120	600	1800
taSMG (m/s^2)	3.372	2.393	0.408	0.196
CR (%)	65.6	75.6	95.8	98.0
Time (s)	3600 (= 1 h)	7200	10800	18000 (= 5 h)
taSMG (m/s^2)	0.157	0.144	0.108	0.121
CR (%)	98.4	98.5	98.9	98.8

*CR: Convergence rate

4.2. Algorithm 2: taSMG with reduced poles

Algorithm 2 was suggested to reduce the pole and generate a more even distribution of gravitational vectors. The angular velocity of Actuator 1 for each latitude θ was controlled as suggested in (2). As represented in Fig. 6, the size and the density of the two poles were significantly reduced compared to those in Algorithm 1. Fig. 7(a) shows the x, y, and z components of the time-averaged simulated gravity. The green lines in Figs. 7(a) and (b) denote the normed gravitational acceleration for 1 and 5 h, respectively. The results are also summarized in Table 3. The time-averaged value approached 0.128 m/s^2 (0.0131 g) after the 5 h operation. According to the figure, no further significant improvement was expected.

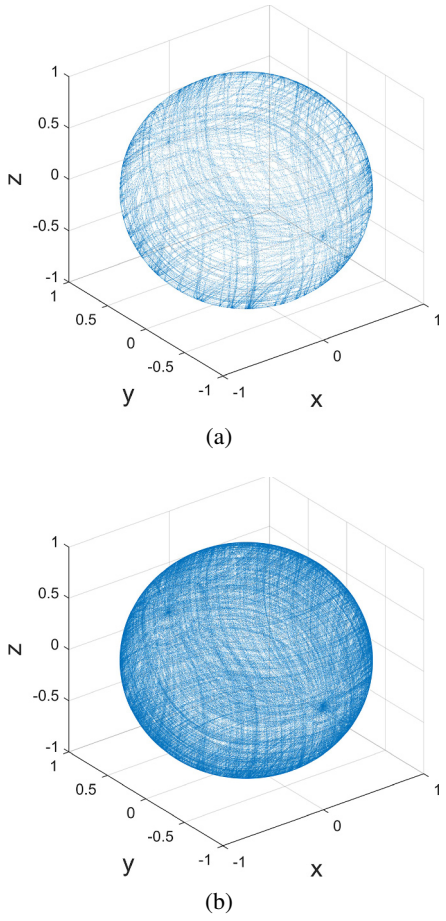

Fig. 6. Gravity distribution generated by Algorithm 2 for (a) 1 h and (b) 5 h.

Table 3. taSMG and convergence rate over time (Algorithm 2).

Time (s)	60	120	600	1800
taSMG (m/s^2)	1.823	1.264	0.180	0.161
CR (%)	81.4	87.1	98.2	98.4
Time (s)	3600 (= 1 h)	7200	10800	18000 (= 5 h)
taSMG (m/s^2)	0.113	0.138	0.128	0.128
CR (%)	98.8	98.6	98.7	98.7

*CR: Convergence rate

4.3. Algorithm 3: taSPG

Algorithm 3 was applied to the 3D clinostat for 5 h. Fig. 8 shows the gravity vector distribution and denotes that the sizes of the two poles were different. Fig. 9(a) illustrates the x, y, and z components of the time-averaged simulated gravity as time passed. The green lines in Figs. 9(a) and (b) depict the normed gravitational acceleration. The results are also summarized in Table 4. The

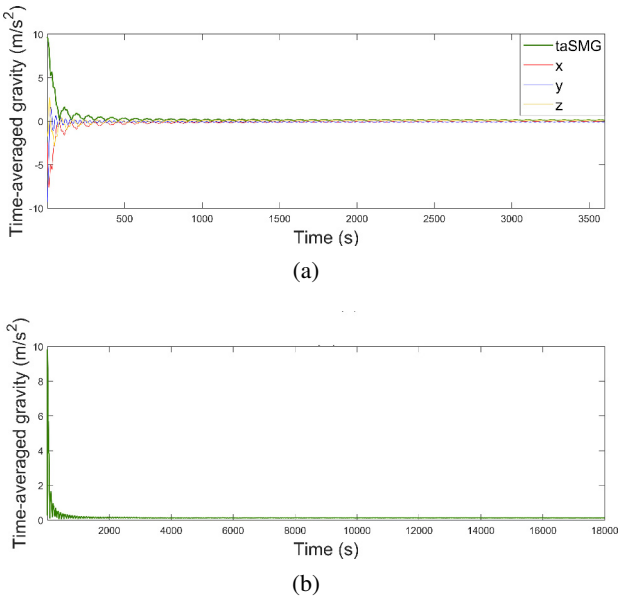

Fig. 7. Time-averaged simulated microgravity generated by Algorithm 2. (a) represents taSMG and its x, y, and z components for 1 h. (b) represents taSMG for 5 h.

Table 4. taSPG and convergence rate over time (Algorithm 3).

Time (s)	60	120	600	1800
taSPG (m/s^2)	5.900	5.268	4.509	4.327
CR (%)	63.2	77.8	95.4	99.7
Time (s)	3600 (= 1 h)	7200	10800	18000 (= 5 h)
taSPG (m/s^2)	4.349	4.360	4.375	4.368
CR (%)	99.2	98.9	98.6	98.7

*CR: Convergence rate

time-averaged value converged to 4.368 m/s^2 (0.446 g) after 5 h. The numerically calculated theoretical value (5) was 4.3125 m/s^2 (0.440 g). These results implied that the 3D clinostat with Algorithm 3 provided the taSPG with a 1.29% error. The taSPG already reached 4.327 m/s^2 (0.34% error) at 30 min, and a little fluctuation in value was observed since then.

The taSPG was generated by the pole position control. Fig. 10(a) shows the pole position error. The pole position converged to almost zero in the form of a damped oscillation. Although the initial pole position had an error of 7.29°, it finally approached zero. From the 35th cycle, the pole position error did not deviate by 1°. Model parameter w_1 also converged to a specific value (Fig. 10(b)) as the pole position error converged to zero. w_1 reached 0.1203 rad/s after the 5 h operation. The initial value was

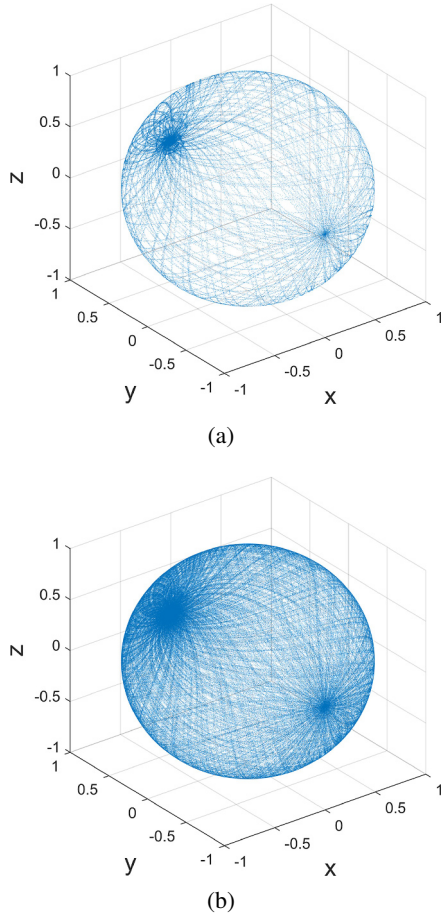

Fig. 8. Gravity distribution generated by Algorithm 3 for (a) 1 h and (b) 5 h.

0.119834 rad/s; hence, an equilibrium point was formed by a 0.39% increase.

5. DISCUSSION

Even though Algorithms 1 and 2 were both effective in generating taSMG, the measured value did not reach below 10^{-3} g indicated in the simulation results of the previous report [16]. In the previous study, the angular velocities of Actuators 1 and 2 were set to 0.913 and 0.683 rpm, respectively. In this study, the mean angular velocities of Actuators 1 and 2, for Algorithm 1, were 0.744 and 1.087 rpm, respectively. The difference between the angular velocities of the previously reported simulation and the current study was not prominent in view of the order of magnitude; hence, the centrifugal force may not be the cause of this difference. It would be due to practical operations of hardware. However, the level of taSMG is within an acceptable range for cell experiments.

The results of Algorithm 2 showed that the size and density of the poles were significantly reduced. However, the small poles still remained because the algorithm lim-

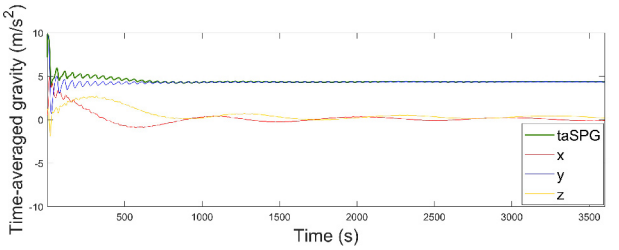

(a)

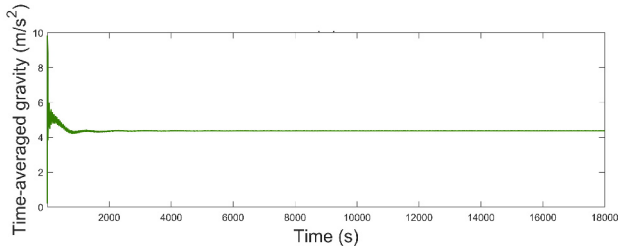

(b)

Fig. 9. Time-averaged simulated partial gravity generated by Algorithm 3. (a) represents taSPG and its x, y, and z components for 1 h. (b) represents taSPG for 5 h.

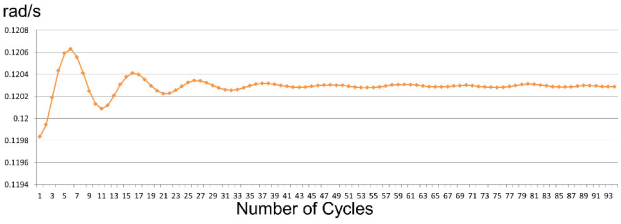

(a)

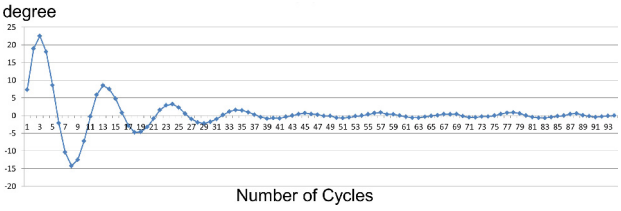

(b)

Fig. 10. (a) Convergence of the model parameter $\boldsymbol{w_1}$. (b) Convergence of the pole position error.

ited the motor angular velocity according to (2). Theoretically, it is ideal to rotate the outer frame with an infinite angular velocity at the center of both poles. However, the practical performance of the actuators has limited conditions, and the focusing of the gravity vectors at poles is inevitable. The higher the maximum angular velocity w_{max} was set, the smaller the pole size. The relative amount of the accumulated gravity vectors for each latitude is shown in the histogram of Figs. 11 and 12 to compare the uniformities of the gravity vector distribution generated by Al-

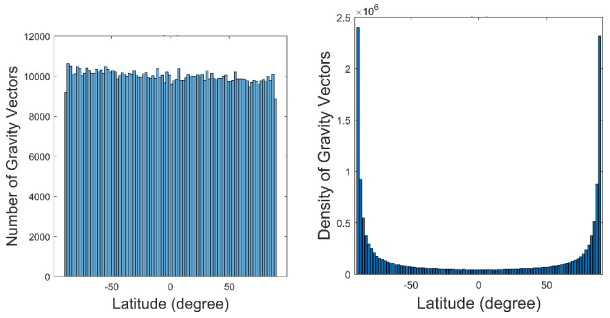

(a) (b)

Fig. 11. Histogram of Algorithm 1 results for 5 h: (a) number of gravity vectors and (b) density of gravity vectors.

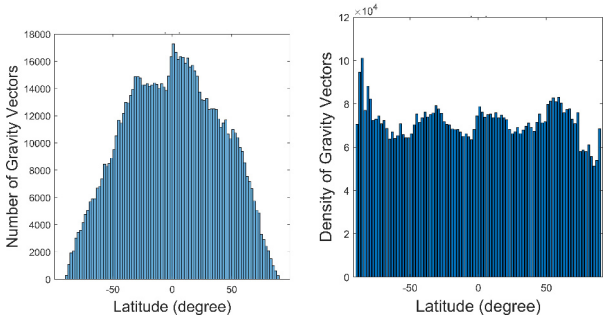

(a) (b)

Fig. 12. Histogram of the Algorithm 2 results for 5 h: (a) number of gravity vectors and (b) density of gravity vectors.

gorithms 1 and 2. As the results of Algorithm 1, Fig. 11(a) shows the number of gravity vectors for a certain latitude, while Fig. 11(b) depicts the density of the gravity vector for a certain latitude (the bin size of latitude was 2° for all histograms). The histogram depicts that the density at both pole regions (latitude $= -90°$ and $90°$) was significantly higher than other regions as a U-shape. However, in Fig. 12(b), the density distribution was relatively even, and the poles were not obviously protruded. This result implied that Algorithm 2 was effective for inducing an even distribution of the gravity vectors compared with conventional Algorithm 1.

taSPG was successfully generated, and the error rate to the goal value was only 1.29%: 30 min was sufficient to reach the goal value with a negligible error. Fig. 13 shows that gravity was focused toward a large pole (latitude$= +90°$), and a small pole shows a smaller gravity concentration. Furthermore, the PD control found the proper w_1 to cancel the limitations of the practical actuator (Fig. 10(a)). Taken together, Algorithm 3 enabled the taSPG to rapidly and stably reach an accurate target gravity value. Future studies will search for optimal control gains to reach various target gravities, with a higher per-

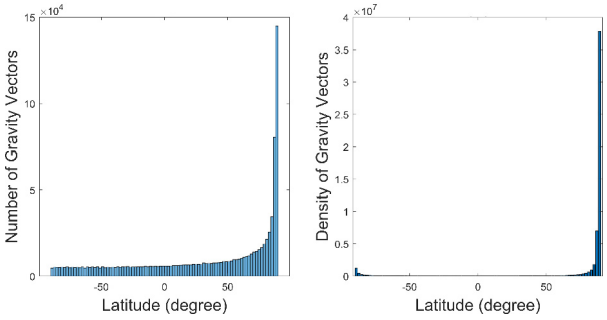

(a) (b)

Fig. 13. Histogram of the Algorithm 3 results for 5 h: (a) number of gravity vectors and (b) density of gravity vectors.

formance.

It was confirmed that Algorithm 3 was able to realize taSPG up to 0.44 g, and it is possible to simulate various gravity values including that of the Moon (0.17 g) or Mars (0.38 g). It is important to search for applications of various gravities to cure and care for diseases in view of space medicine. However, Algorithm 3 cannot generate taSPG above 0.44 g in its current state. α was set to 1; hence, a larger taSPG value cannot be realized. Instead, two alternative approaches can be considered. First, α larger than 1 can be allowed even though w has a negative value near the large pole. However, it does not matter physically that w has a negative value, indicating rotation in the opposite direction. Second, the outer frame rotation can stop for a while to enhance the large pole. At parameter $\alpha = 1$, the outer frame rotation momentarily stopped at the large pole without discontinuity. The imbalance between the two poles can be further strengthened by extending the stationary time.

Algorithms 2 and 3 were advantageous in predicting the convergence of gravity values over time, given that the latitude of the gravity vector was controlled by a mathematical model instead of total randomness. In the previously reported random walk algorithm for uniform taSMG and taSPG, the gravity vector changed to an arbitrary random direction [19] to avoid a predictable trajectory. Although the random variation of the trajectory highly supported the more controlled results of cell cultivation, the convergence time for a time-averaged gravity value was not guaranteed. Thus, the control signal should be recorded to provide a consistent convergence time when the same cell cultivations were repeated. In addition, a discontinuously varying velocity profile from the random walk algorithm led to momentary impact, which can cause the accumulation of acceleration and irregularity of gravity patterns. On the other hand, accurate convergence time can be predicted as the latitude was controlled based on a mathematical model. Controlling the gravity vector based on the model can prevent the gravity vector from wandering at an unnecessary position for the convergence of time-averaged gravity values, thus reducing the convergence time to reach taSMG and taSPG. Furthermore, the longitude of the gravity vector was controlled based on angular velocity with random distribution, and the randomness of the gravity vector trajectory was also guaranteed.

For future study, mechanical hardware should be improved for expanded conditions. The 3D clinostat mostly requires control with low actuator velocities to minimize non-gravitational accelerations (including centrifugal acceleration) [16]. In particular, centrifugal acceleration caused by high angular velocity of Algorithm 2 can affect cell growth and should be further decreased to minimized unwanted effects. Thus, the unused high-speed region can be utilized to increase the angular velocity increment resolution of the low-speed region, by applying a gear system. The 3D clinostat with an improved gear system will contribute to the performance enhancement of the suggested algorithms.

6. CONCLUSION

This study designed two novel algorithms for simulating micro- and partial gravity. For validation, 3D clinostat hardware with high durability was developed and operated by designed algorithms. Compared to the conventional Algorithm 1, Algorithm 2 was able to generate a more evenly distributed gravity vector with reduced poles. Algorithm 3 generated taSPG with a measured value that almost converged to the analytically calculated value. Suggested Algorithms 2 and 3 were based on a mathematical model, so the convergence pattern of time-averaged gravity can be predicted and the unintended accumulation of acceleration, by abrupt rotating changes, can be reduced. Using the developed 3D clinostat hardware and algorithms in this study, highly controlled cell growth experiments in taSMG and taSPG can be effectively conducted for the study of space medicine.

REFERENCES

[1] R. H. Fitts, S. W. Trappe, D. L. Costill, P. M. Gallagher, A. C. Creer, P. A. Colloton, J. R. Peters, J. G. Romatowski, J. L. Bain, and D. A. Riley, "Prolonged space fight-induced alterations in the structure and function of human skeletal muscle fibres," *The Journal of Physiology*, vol. 588, no. 18, pp. 3567-3592, September 2010.

[2] D. A. Riley, J. L. Bain, J. L. Thompson, R. H. Fitts, J. J. Widrick, S. W. Trappe, T. A. Trappe, and D. L. Costill, "Decreased thin filament density and length in human atrophic soleus muscle fibers after space flight," *Journal of Applied Physiology*, vol. 88, no. 2, pp. 567-572, February, 2000.

[3] S. W. Trappe, T. A. Trappe, G. A. Lee, J. J. Widrick, D. L. Costill, and R. H. Fitts, "Comparison of a space shuttle

fight (STS-78) and bed rest on human muscle function," *Journal of Applied Physiology*, vol. 91, no. 1, pp. 57-64, July 2001.

[4] K. M. Baldwin, R. E. Herrick, E. Ilyina-Kakueva, and V. S. Oganov, "Effects of zero gravity on myofibril content and isomyosin distribution in rodent skeletal muscle," *The FASEB Journal*, vol. 4, no. 1, pp. 79-83, January 1990.

[5] M. L. Lewis, J. L. Reynolds, L. A. Cubano, J. P. Hatton, B. D. Lawless, and E. H. Piepmeier, "Space flight alters microtubules and increases apoptosis in human lymphocytes (Jurkat)," *The FASEB Journal*, vol. 12, no. 11, pp. 1007-1018, August 1998.

[6] D. Williams, A. Kuipers, C. Mukai, and R. Thirsk, "Acclimation during space flight: Effects on human physiology," *Canadian Medical Association Journal*, vol. 180, no. 13, pp. 1317-1323, June 2009.

[7] S. K. Mehta, R. P. Stowe, A. H. Feiveson, S. K. Tyring, and D. L. Pierson, "Reactivation and shedding of cytomegalovirus in astronauts during space flight," *The Journal of Infectious Diseases*, vol. 182, no. 6, pp. 1761-1764, November 2000.

[8] J. B. Boonyaratanakornkit, A. Cogoli, C. F. Li, T. Schopper, P. Pippia, G. Galleri, M. A. Meloni, and M. Hughes-Fulford, "Key gravity sensitive signalling pathways drive T cell activation," *The FASEB Journal*, vol. 19, no. 14, pp. 2020-2022, October 2005.

[9] A. Villa, S. Versari, J. A. Maier, and S. Bradamante, "Cell behavior in simulated microgravity: A comparison of results obtained with RWV and RPM," *Gravitational and Space Biology Bulletin*, vol. 18, no. 2, pp. 89-90, June 2005.

[10] J. P. Hatton, F. Gaubert, M. L. Lewis, Y. Darsel, P. Ohlmann, J. P. Cazenave, and D. Schmitt, "The kinetics of translocation and cellular quantity of protein kinase C in human leukocytes are modified during spaceflight," *The FASEB Journal*, vol. 13, no. 9001, pp. 23-33, May 1999.

[11] M. Cogoli-Greuter, "The lymphocyte story - An overview of selected highlights on the in vitro activation of human lymphocytes in space," *Microgravity Science and Technology*, vol. 25, no. 6, pp. 343-352, July 2014.

[12] M. Schwarzenberg, M. A. Meloni, G. Cossu, M. Cogoli-Greuter, and A. Cogoli, "Signal transduction in T lymphocytesA comparison of the data from space, the free fall machine and the random positioning machine," *Advances in Space Research*, vol. 24, no. 6, pp. 793-800, February 1999.

[13] I. Walther, P. Pippia, M. A. Meloni, F. Turrini, F. Mannu, and A. Cogoli, "Simulated microgravity inhibits the genetic expression of interleukin-2 and its receptor in mitogen-activated T lymphocytes," *FEBS Letters*, vol. 436, no. 1, pp. 115-118, September 1998.

[14] J. W. A. van Loon, "Some history and use of the random positioning machine, RPM, in gravity related research," *Advances in Space Research*, vol. 39, no. 7, pp. 1161-1165, 2007.

[15] A. G. Borst, and J. W. A. van Loon, "Technology and developments for the random positioning machine, RPM," *Microgravity Science and Technology*, vol. 21, no. 287, pp. 287-292, November 2009.

[16] Y. J. Kim, A. J. Jeong, M. J. Kim, C. W. Lee, S.-K. Ye, and S. Kim, "Time-averaged simulated microgravity (taSMG) inhibits proliferation of lymphoma cells, L-540 and HDLM-2, using a 3D clinostat," *BioMedical Engineering OnLine*, vol. 16, no. 48, pp. 1-12, April 2017.

[17] A. J. Jeong, Y. J. Kim, M. H. Lim, H. Lee, K. Noh, B.-H. Kim, J. W. Chung, C.-H. Cho, S. Kim, and S.-K. Ye, "Microgravity induces autophagy via mitochondrial dysfunction in human Hodgkin's lymphoma cells," *Scientific Reports*, vol. 8, no. 14646, pp. 1-10, October 2018.

[18] S. L. Wuest, S. Richard, I. Walther, R. Furrer, R. Anderegg, J. Sekler, and M. Egli, "A novel microgravity simulator applicable for three-dimensional cell culturing," *Microgravity Science and Technology*, vol. 26, no. 2, pp. 77-88, October 2014.

[19] A. Manzano, R. Herranz, L. A. den Toom, S. te Slaa, G. Borst, M. Visser, F. J. Medina, and J. W. A. van Loon, "Novel, Moon and Mars, partial gravity simulation paradigms and their effects on the balance between cell growth and cell proliferation during early plant development," *npj Microgravity*, vol. 4 no. 9, pp. 1-11, 2018.

[20] A. Rojas-Moreno, and F. Santos-Rodriguez, "Design of a novel 3DOF clinostat to produce microgravity for bioengineering applications," *Proc. of the IEEE XXV International Conference on Electronics, Electrical Engineering and Computing (INTERCON)*, August 2018.

Yoon Jae Kim received his B.S. degree in Mechanical & Aerospace Engineering and his Ph.D. degree in Interdisciplinary Program for Bioengineering from Seoul National University (SNU), in 2014 and 2018, respectively. He is a post-doctoral researcher with the Institute of Medical and Biological Engineering, SNU since Nov. 2018. His research interests include medical robot, machine learning, and biosignal processing.

Min Hyuk Lim received his B.S. degree in Physics, M.D. in medicine, and M.S. degree in medicine (Biomedical Engineering) from Seoul National University (SNU), in 2007, 2011, and 2016, respectively. He is a Ph.D. student in medicine (Biomedical Engineering) of SNU and a medical doctor in Department of Biomedical Engineering in Seoul National University Hospital. His research interests are optimization and control theory combined with machine learning for biomedical fields.

Byoungjun Jeon received his B.S. degree in Biophysics from University of Washington in 2014. He is currently pursuing a Ph.D. degree in the Interdisciplinary Program for Bioengineering from Seoul National University. His research interests include medical robot, biological physics, microfluidics.

Dong Hyun Choi received his M.D. and B.S. degrees in medicine from Seoul National University, Seoul Korea in 2016. He is currently pursuing an M.S. degree in medicine from Seoul National University.

Haeri Lee received her B.S. degree in Biochemistry and Cell biology from The State University of New York at Stony Brook in 2011. She is a Ph.D. student in Pharmacology and Biomedical Sciences from Seoul National University College of Medicine. Her research interests include cancer, tumor microenvironment and immune-oncology.

Ae Jin Jeong received her B.S. and M.S. degrees in Bioscience from Dong-A University, in 2012 and 2014, respectively. She is a Ph.D. student in Pharmacology and Biomedical Sciences from Seoul National University College of Medicine. Her research interests include immune-oncology, cancer and NK therapy.

Min Jung Kim received her M.D. and B.S degree in medicine from Seoul National University, Seoul, Korea in 2007, and an M.S. degree in medicine from SNU in 2014. She is currently pursuing a Ph.D. degree in medicine from Seoul National University and a clinical assistant professor with the Department of Surgery in Seoul National University Hospital since 2018. Prior to joining to the Seoul National University Hospital, she worked as a staff surgeon at National Cancer Center, Goyang, Korea.

Ji Won Park received his M.D. and B.S degrees in medicine from Seoul National University, Seoul, Korea in 2001, and his M.S. degree and Ph.D. degree in medicine from Chungbuk National University, Cheongju, Korea, in 2008 and 2019, respectively. He has been a clinical associate professor at the Department of Surgery, Seoul National University Hospital since 2013. Prior to joining to the Seoul National University Hospital, he worked as a staff surgeon at National Cancer Center, Goyang, Korea.

Ja-Lok Ku received his B.S, M.S., Ph.D. degrees in veterinary medicine from Seoul National University (SNU), Seoul, Korea, in 1992, 1994, and 1998, respectively. He is a professor with the Department of Biomedical Sciences and Laboratory of Cell Biology, Cancer Research Institute, Seoul National University College of Medicine since 2001. He is also a principal investigator for Korean Cell Line Bank (KCLB), Seoul, Korea.

Seung-Yong Jeong received his M.D. and B.S. degrees in medicine from Seoul National University, Seoul, Korea, in 1989, and his M.S. degree and Ph.D. degree in medicine from Seoul National University, in 1999 and 2001, respectively. He has been a professor at the Department of Surgery, Seoul National University College of Medicine since 2013. Prior to joining to the Seoul National University, he worked as a Head of Center for Colorectal Cancer and a Director of Research Institute for Colorectal Cancer in National Cancer Center, Goyang, Korea.

Sang-Kyu Ye received his B.S degree in Molecularbiology and M.S. degree in Microbiology (Kwang Ho Lee Lab. Molecular Immunology) from Kon-kuk University, Korea in 1994 and 1996, and his Ph.D. degree in Medical Science (Tasuku Honjo Lab. Immunology) from Kyoto University, Japan in 2001. After working as a postdoctoral fellowship at the Institute for Virus Research Kyoto University (Koich Ikuta Lab, JSPS fellowship, Japan), he was appointed as an assistant professor of Department of Pharmacology, Seoul National University College of Medicine in 2002. He was promoted to Full Professor in 2011. Dr. Ye's laboratory, Cancer Stem Cells & Tumor Microenvironment, has been studying roles of STAT3 in cancer cells, especially their oncogenic and metastatic activity.

Youdan Kim received his B.S. and M.S. degrees in aeronautical engineering from Seoul National University, Korea, and his Ph.D. degree in aerospace engineering from Texas A&M University, in 1983, 1985, and 1990, respectively. He joined the faculty of the Seoul National University in 1992, where he is currently a Professor in the Department of Mechanical and Aerospace Engineering. His current research interests include the control system design for aircraft and spacecraft, aerial robot system, and medical robot system.

Sungwan Kim received his B.S degree in Electronics Engineering and M.S. degree in Control & Instrumentation Engineering from Seoul National University (SNU), Seoul, Korea, in 1985 and 1987, and his Ph.D. degree in Electrical Engineering from University of California at Los Angeles in 1993, respectively. He is a professor with the Department of Biomedical Engineering, SNU College of Medicine since 2010. Prior to joining to the SNU, he worked as a Senior Aerospace Engineer at National Aeronautics and Space Administration (NASA) Langley Research Center, Hampton, Virginia, USA. He is an Associate Fellow of the AIAA and a Senior Member of the IEEE.